

NANO EXPRESS

Open Access



Experimental Research on Stability and Natural Convection of TiO₂-Water Nanofluid in Enclosures with Different Rotation Angles

Cong Qi*, Guiqing Wang, Yifeng Ma and Leixin Guo

Abstract

The stability and natural convection heat transfer characteristics of TiO₂-water nanofluid in enclosures with different rotation angles ($\alpha = -45^\circ$, $\alpha = 0^\circ$, $\alpha = 45^\circ$, and $\alpha = 90^\circ$) are experimentally investigated. The effects of different pH values and doses (m) of dispersant agent on the stability of TiO₂-water nanofluid are investigated. It is found that TiO₂-water nanofluid with $m = 6$ wt% and pH = 8 has the lowest transmittance and has the best stability. The effects of different rotation angles ($\alpha = -45^\circ$, $\alpha = 0^\circ$, $\alpha = 45^\circ$, and $\alpha = 90^\circ$), nanoparticle mass fractions (wt% = 0.1%, wt% = 0.3%, and wt% = 0.5%) and heating powers ($Q = 1$ W, $Q = 5$ W, $Q = 10$ W, $Q = 15$ W, and $Q = 20$ W) on the natural convection heat transfer characteristics are also studied. It is found that the enclosure with rotation angle $\alpha = 0^\circ$ has the highest Nusselt number, followed by the enclosure with rotation angles $\alpha = 45^\circ$ and $\alpha = 90^\circ$, the enclosure with rotation angle $\alpha = -45^\circ$ has the lowest Nusselt number. It is also found that natural convection heat transfer performance increases with the nanoparticle mass fraction and heating power, but the enhancement ratio decreases with the heating power.

Keywords: Natural convection, Nanofluid, Rotation angle, Stability

Background

Since nanofluid is prepared, due to its excellent heat conducting properties [1–3], nanofluid is widely applied in heat transfer field [4–6], especially in the natural convection field [7–9].

Natural convection heat transfer characteristics of nanofluid are numerically investigated by many researchers. He et al. [10, 11] applied a single-phase and a two-phase lattice Boltzmann methods to numerically study the natural convection heat transfer of Al₂O₃-water nanofluid in a square cavity, respectively. Sheikholeslami et al. [12] investigated the magnetohydrodynamic natural convection heat transfer characteristics of a horizontal cylindrical enclosure with an inner triangular cylinder filled with Al₂O₃-water nanofluid by a lattice Boltzmann simulation method. Uddin et al. [13] studied the natural convection heat transfer of various nanofluids along a vertical plate

embedded in porous medium based on the Darcy-Forchheimer model. Meng et al. [14] numerically investigated the natural convection of a horizontal cylinder filled with Al₂O₃-water nanofluid. Ahmed et al. [15] used a two-phase lattice Boltzmann method to study the natural convection of CuO-water nanofluid in an inclined enclosure. Qi et al. [16] numerically simulated the natural convection of Cu-Ga nanofluid in an enclosure.

In addition to above numerical simulations on the natural convection of nanofluid, the experimental studies on natural convection of nanofluid are done by more and more researchers. Li et al. [17] experimentally investigated the natural convection heat transfer of ZnO-EG/water nanofluid. Hu et al. [18, 19] experimentally studied the natural convection heat transfer enhancement of a square enclosure filled with TiO₂-water and Al₂O₃-water nanofluids respectively. Ho et al. [20] experimentally studied the natural convection heat transfer of vertical square enclosures with different sizes filled with Al₂O₃-water nanofluid. Heris et al. [21–23] experimentally

* Correspondence: qicong@cumt.edu.cn
School of Electrical and Power Engineering, China University of Mining and Technology, 221116 Xuzhou, China

investigated the convective heat transfer characteristics of different kinds of nanofluid (Cu/water, Al₂O₃-water, and CuO-water) in circular tubes, respectively. Mansour et al. [24] experimentally investigated the mixed convection of an inclined tube filled with Al₂O₃-water nanofluid. Chang et al. [25] experimentally investigated the natural convection of Al₂O₃-water nanofluid

in thin enclosures. Wen et al. [26, 27] experimentally investigated the convective heat transfer characteristics of Al₂O₃-water nanofluids and TiO₂-water nanofluids under laminar flow conditions, respectively. Xuan et al. [28] experimentally studied the convection heat transfer of Cu-water nanofluid in a straight brass tube.

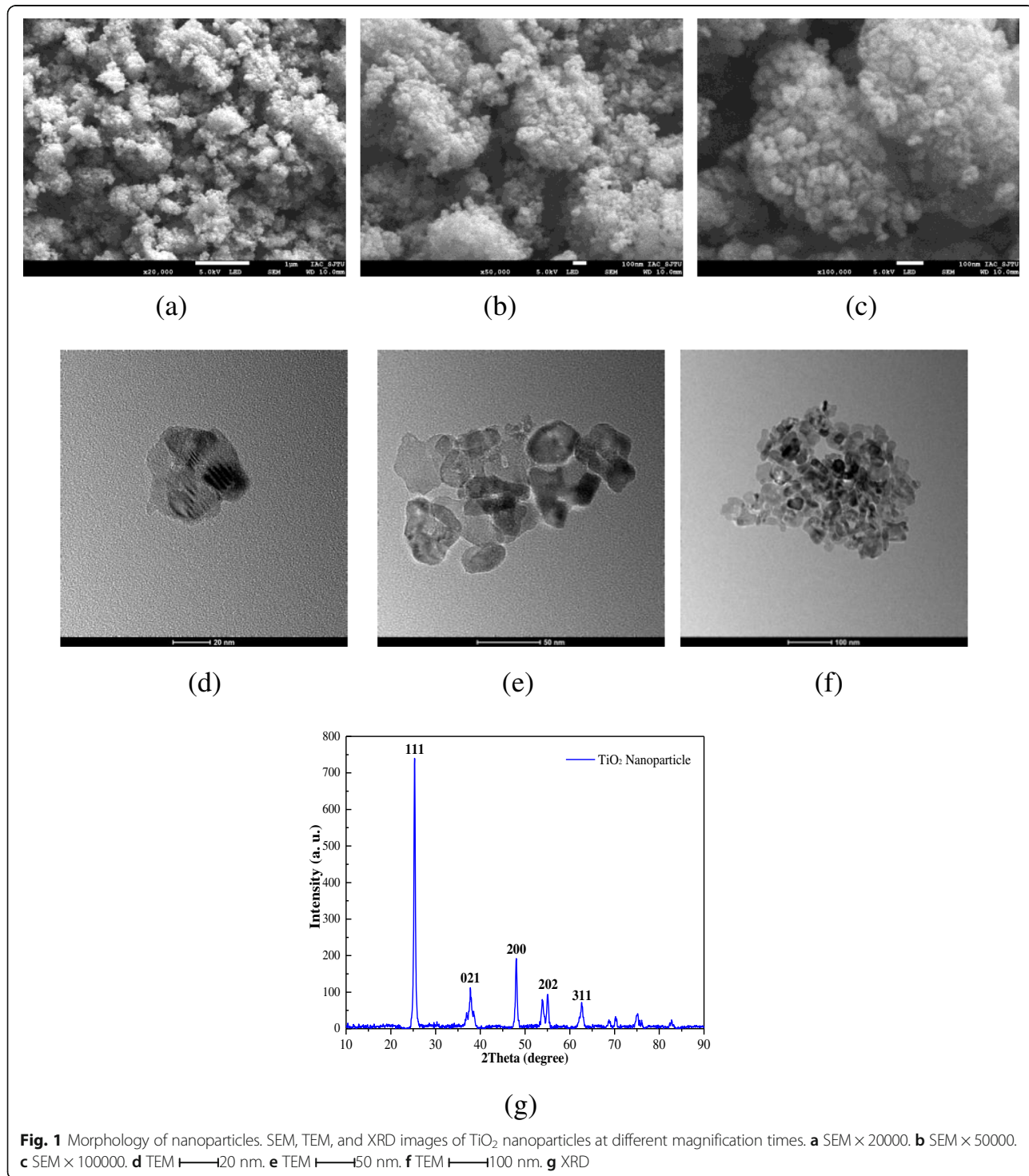


Fig. 1 Morphology of nanoparticles. SEM, TEM, and XRD images of TiO₂ nanoparticles at different magnification times. **a** SEM × 20000. **b** SEM × 50000. **c** SEM × 100000. **d** TEM ——— 20 nm. **e** TEM ——— 50 nm. **f** TEM ——— 100 nm. **g** XRD

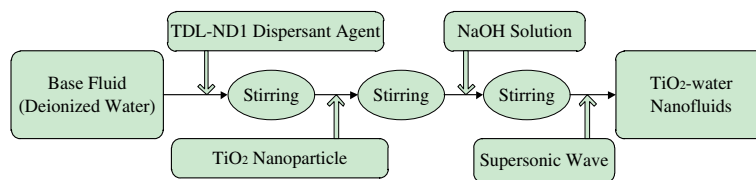


Fig. 2 Preparation of nanofluids. Preparation procedure of TiO₂-water nanofluids by a two-step method

Above literatures made a great contribution in the natural convection heat transfer characteristics of nanofluid. However, the natural convection heat transfer enhancement of enclosures with different rotation angles filled with nanofluid is needed to be investigated further. Hence, the stability and natural convection heat transfer characteristics of TiO₂-water nanofluid in enclosures with different rotation angles ($\alpha = -45^\circ$, $\alpha = 0^\circ$, $\alpha = 45^\circ$, and $\alpha = 90^\circ$) are experimentally investigated in this paper.

Method

Preparation of Nanofluid and its Stability

TiO₂ is chosen as the nanoparticles. Figure 1 presents the SEM, TEM, and XRD images of TiO₂ nanoparticles at different magnification times. It can be found that from SEM images that the nanoparticles easily gather together, and it is necessary to take some measures to prepare the stable nanofluids. It can be also found that from TEM images that the particle size is about 10 nm, and the shapes of nanoparticles are flat. Flat nanoparticles have a larger heat transfer area than spherical nanoparticles at the same mass fraction, which is advantageous to heat transfer enhancement. Figure 1g shows the XRD patterns of the TTP-A10 TiO₂ nanoparticle. As observed, the strong and sharp peaks suggest that

the TTP-A10 TiO₂ nanoparticle sample is highly crystalline. The average particle size of the sample can be calculated by the Scherrer equation presented in Eq. (1). The TiO₂ nanoparticle sizes are 6, 9, 14, 20, and 35 nm calculated by these diffraction peak values (111, 200, 021, 202, and 311), and the smallest nanoparticle sizes are about 6 and 9 nm based on the diffraction peak values (111 and 200). The big nanoparticle sizes may be caused by the aggregation of nanoparticles. The smallest values (6 and 9 nm) may be the real sizes of nanoparticle, the size of a few nanoparticles may be 6 nm, and most nanoparticle sizes may be about 9 nm, which are more close to the description supplied by the manufacturer (10 nm) and the TEM images (10 nm).

$$D_c = \frac{k\lambda}{\beta \cdot \cos\theta} \tag{1}$$

where k is the value for the shape factor, and $k = 0.9$; λ is the X-ray wavelength; and β is the line broadening full width at half maximum (FWHM) of peak height in radians, and θ is the Bragg diffraction angle.

TiO₂-water nanofluid with different nanoparticle mass fractions (wt% = 0.1%, wt% = 0.3%, and wt% = 0.5%) is

Table 1 Information of materials and equipments. Information of some materials and equipments in the preparation of nanofluids

Materials and equipments	Manufacturer	Properties
TiO ₂ nanoparticles	Nanjing Tansail Advanced Materials Co., Ltd.	Type: TTP-A10; Crystal form: anatase; Particle diameter:10 nm
Base fluid (deionized water)	Prepared by ultrapure water device	Resistivity: 16–18.2 MΩ·cm@25 °C
Ultrapure water device	Nanjing Yeap Esselte Technology Development Co., Ltd.	Type: EPED-E2-10TJ
Dispersant agent	Nanjing Tansail Advanced Materials Co., Ltd.	Type: TDL-ND1; Element: macromolecule polymers; Scope of application: water or solvent (base fluid)
Ultrasonic oscillation device	Shenzhen Jeken Ultrasonic Technology Co., Ltd.	Type: PS-100A; Ultrasonic frequency: 40,000 HZ
Magnetic stirring apparatus	Shanghai MeiYingPu Instrument Manufacturing Co., Ltd.	Type: MYP11-2 Rotate speed: 50 ~ 1500 r/min
Electronic analytical balance	Shanghai Hengping Instrument and Meter Factory	Type: FA2204; Precision: 0.1 mg

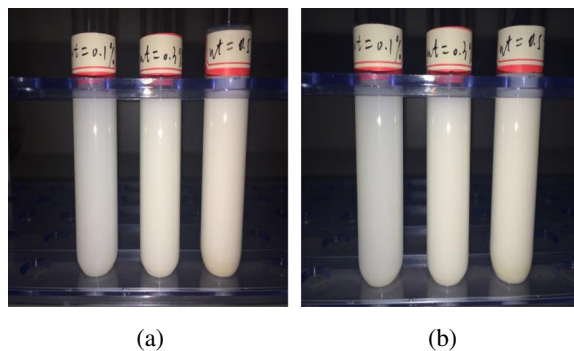


Fig. 3 Stability observation of TiO₂-water nanofluid. TiO₂-water nanofluid at different times. **a** Before laying. **b** After 72 h

prepared by the two-step method, which is shown in Fig. 2. Mechanical stirring time is half an hour for each of the sub-steps, and the sonication time is 40 min. Table 1 shows the information of some materials and equipments in the preparation of nanofluids. Figure 3 shows the TiO₂-water nanofluid before laying and after 72 h. It can be seen that there is little deposition of nanoparticles in the test tube and nanofluid prepared in this paper shows a good stability.

In addition to the study on whether there is deposition of nanoparticles in the test tube, the effects of transmittance (τ) of nanofluid on its stability are also discussed.

Figure 4 gives the transmittance (τ) changes of TiO₂-water nanofluid (wt% = 0.5%) with different pH values and doses (m) of dispersant agent. The transmittance is measured by an ultra violet visible spectrophotometer (UV-1800(PC)). As we know, if the nanoparticles uniformly distribute in the water, the nanoparticles will reflect the most light and have a high reflectance (a low transmittance). Hence, the stability of nanofluid is inversely proportional to the transmittance, and the stable nanofluid has a low transmittance. It can be found from Fig. 4 that the nanofluid with $m = 6$ wt% and pH = 8 has the lowest transmittance and

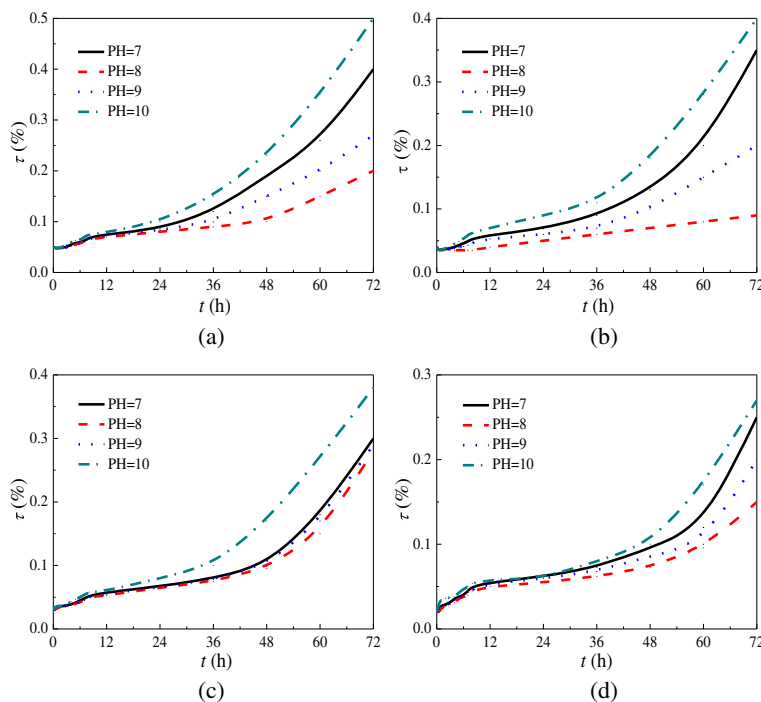
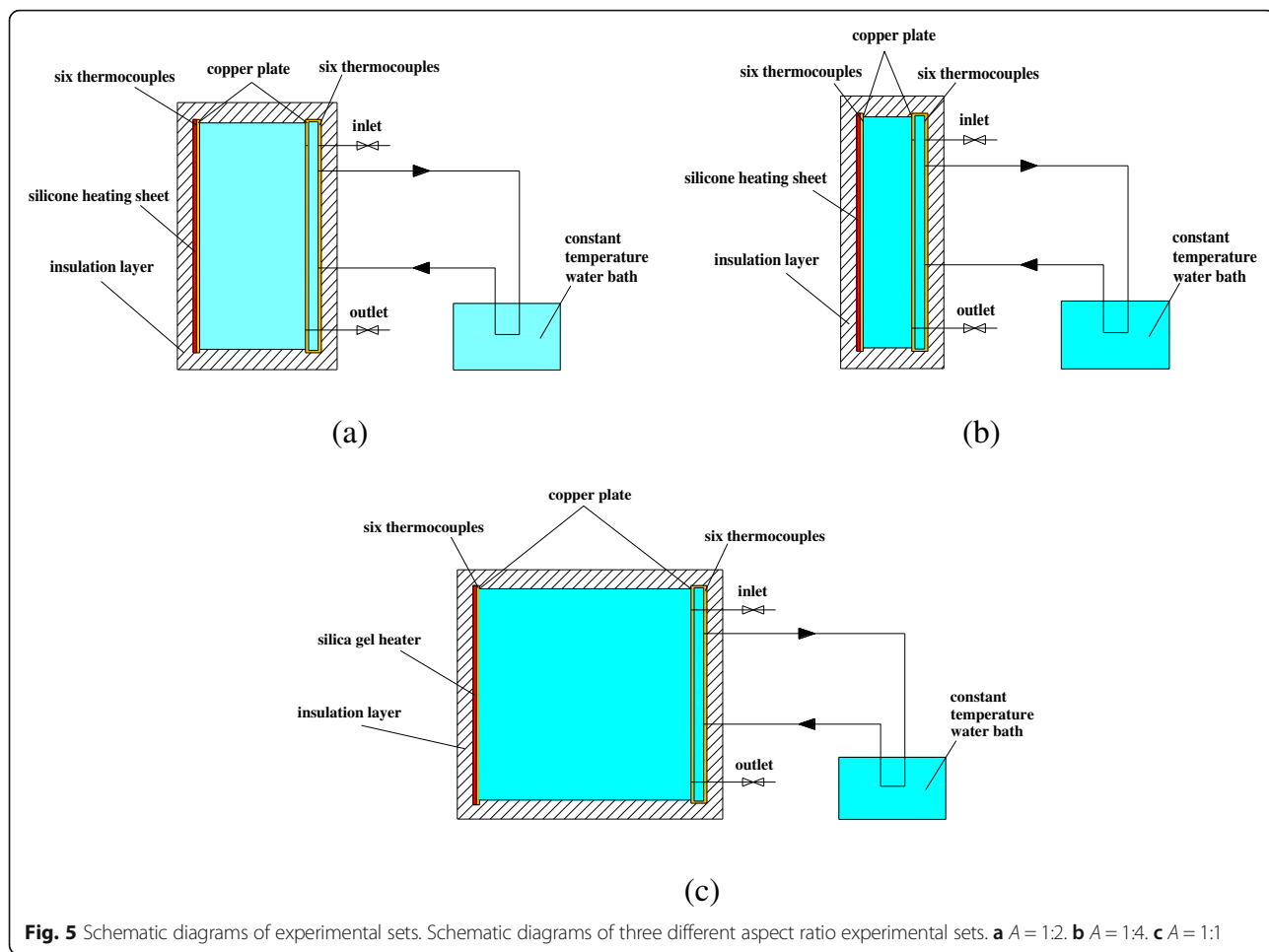


Fig. 4 Transmittance of TiO₂-water nanofluid. Transmittance (τ) changes of TiO₂-water nanofluid (wt% = 0.5%) under different pH values with times (t) at different doses (m) of dispersant agent. **a** $m = 5$ wt%. **b** $m = 6$ wt%. **c** $m = 7$ wt%. **d** $m = 8$ wt%

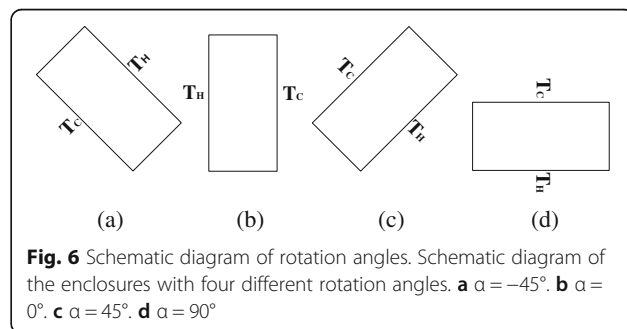


has the best stability. The nanofluids with different nanoparticle mass fractions in this experiment are prepared at $m = 6$ wt% and $\text{pH} = 8$, which can ensure the stability of nanofluids.

Experimental System

Figure 5 shows the schematic diagrams of the three experimental sets. The sizes of the three rectangular enclosures are 10 cm (width) \times 20 cm (height), 5 cm (width) \times 20 cm (height), and 20 cm (width) \times 20 cm (height). The width and height are defined as W and H , respectively, and the aspect ratio (A) of the enclosure is defined as $A = W / H$. The left wall (copper plate) of the enclosure is heated by a silicone heating sheet connected to a DC power. The right wall (copper plate) of the enclosure is cooled by the cooling water in a small cavity (the material is also copper) connected to a constant temperature water bath. The temperatures of two sides of the enclosure are obtained by six thermocouples connected to a data acquisition instrument (Agilent 34972A). The outside insulation layer is used to prevent the heat losing.

The natural convection heat transfer characteristics of the two enclosures with different rotation angles ($\alpha = -45^\circ$, $\alpha = 0^\circ$, $\alpha = 45^\circ$, and $\alpha = 90^\circ$) filled with TiO_2 -water nanofluid are investigated in this paper. For the enclosure with $\alpha = -90^\circ$, the top wall is the hot wall and the bottom wall is the cold wall, and the heat transfer in the enclosure is mainly heat conduction. However, the manuscript mainly investigates the natural convection heat transfer of nanofluid in the enclosure, hence, the enclosure with $\alpha = -90^\circ$ is not considered in



this manuscript. Figure 6 shows the schematic diagram of enclosures with different rotation angles.

Data Processing

The power Q provided by the silicone heating sheet is as follows:

$$Q = UI \tag{2}$$

where U and I are the voltage and electricity of the DC power respectively.

The effective power Q_{net} is as follows:

$$Q_{net} = Q - Q_{loss} \tag{3}$$

where Q_{loss} is the heat loss measured by a heat flow meter.

The temperature of copper plate side next to silicone heating sheet T_H^* is as follows:

$$T_H^* = \frac{(T_1 + T_2 + \dots + T_6)}{6} \tag{4}$$

where T_1, T_2, \dots, T_6 are the temperatures of thermocouples.

The temperature of copper plate side (left side of enclosure) next to nanofluid T_H is as follows:

$$T_H = T_H^* - \frac{Q_{net}\delta}{A\lambda_w} \tag{5}$$

where $\delta = 0.005m$ is the thickness of the copper plate, A is the area of the copper plate, λ_w is the thermal conductivity of the copper plate.

The temperature of copper plate side (right side of enclosure) next to insulation layer T_C is as follows:

$$T_C^* = \frac{(T_7 + T_8 + \dots + T_{12})}{6} \tag{6}$$

where T_7, T_8, \dots, T_{12} are the temperatures of thermocouples in the right side of the enclosure.

When the thermal equilibrium state is reached, the temperature of cooling water is the same with the temperature of the copper plate side next to the cooling water. The temperature of the copper plate side (right

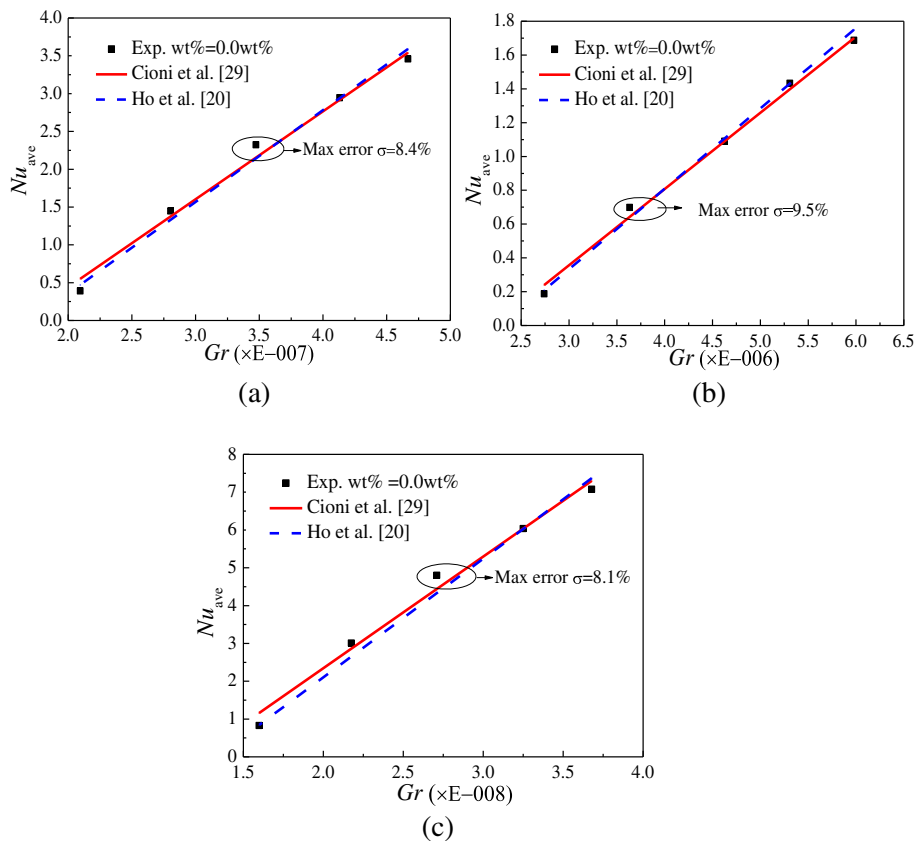


Fig. 7 Experiment set validation. Comparison of Nusselt numbers between the experimental results and the published literatures in enclosures with two different aspect ratios. **a** $A = 1:2$. **b** $A = 1:4$. **c** $A = 1:1$

side of enclosure) next to nanofluid T_C can be calculated as follows:

$$T_C = T_C^* - \frac{2Q_{net}\delta}{A\lambda_w} \tag{7}$$

The qualitative temperature T_m is defined as follows:

$$T_m = \frac{T_H + T_C}{2} \tag{8}$$

The convective heat transfer coefficient h is as follows:

$$h = \frac{Q_{net}}{A(T_H - T_C)} \tag{9}$$

Nusselt number is defined as follows:

$$Nu = \frac{h \cdot W}{\lambda_f} \tag{10}$$

where λ_f is the thermal conductivity of the fluid in the enclosure.

Uncertainty Analysis

The error transfer formula of the convective heat transfer coefficient is as follows [19]:

$$\begin{aligned} \frac{\Delta h}{h} &= \left| \frac{\partial \ln h}{\partial Q_{net}} \right| \Delta Q_{net} + \left| \frac{\partial \ln h}{\partial A} \right| \Delta A + \left| \frac{\partial \ln h}{\partial (T_H - T_C)} \right| \Delta (T_H - T_C) \\ &= \frac{\Delta Q_{net}}{Q_{net}} + \frac{\Delta A}{A} + \frac{\Delta (T_H - T_C)}{(T_H - T_C)} \end{aligned} \tag{11}$$

The error transfer formula of Nusselt number is as follows [19]:

$$\begin{aligned} \frac{\Delta Nu}{Nu} &= \left| \frac{\partial \ln Nu}{\partial h} \right| \Delta h + \left| \frac{\partial \ln Nu}{\partial W} \right| \Delta W + \left| \frac{\partial \ln Nu}{\partial \lambda_f} \right| \Delta \lambda_f \\ &= \frac{\Delta h}{h} + \frac{\Delta W}{W} + \frac{\Delta \lambda_f}{\lambda_f} \end{aligned} \tag{12}$$

Based on the Eqs. (10) and (11), the errors of the convective heat transfer coefficient and Nusselt number are 5.65 and 6.34%, respectively, in this experiment. It can be found that the errors of the experimental sets are

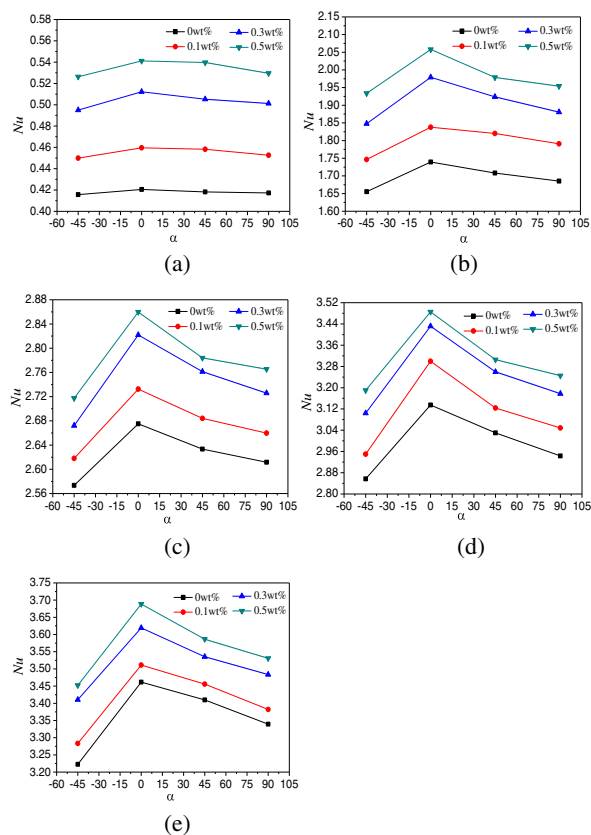


Fig. 8 Changes of Nusselt numbers with rotation angles ($A = 1:2$). Average Nusselt numbers change of nanofluid with rotation angles of enclosure ($A = 1:2$) at different heating powers. **a** $Q = 1$ W. **b** $Q = 5$ W. **c** $Q = 10$ W. **d** $Q = 15$ W. **e** $Q = 20$ W

small, which can ensure the reliability and accuracy of the experimental results.

Results and Discussions

Experiment Validation

Before the study on nanofluid, the experiment validation is necessary. Figure 7 shows the comparison of Nusselt numbers between the experimental results of water and the results of published literatures for enclosures with $A = 1:2$, $A = 1:4$, and $A = 1:1$. The max errors for enclosures with $A = 1:2$, $A = 1:4$, and $A = 1:1$ are 8.4, 9.5, and 8.1%, respectively. It can be found that the experimental results have a good agreement with the results of published literatures [20, 29], which verifies the accuracy and reliability of the experimental system.

Enclosure with $A = 1:2$

The effects of rotation angles on the natural convection heat transfer characteristics of TiO_2 -water nanofluid are discussed in this paper. Figure 8 presents the changes of average Nusselt numbers with the rotation angles of enclosure with $A = 1:2$. It can be found from Fig. 8 that Nusselt numbers firstly increase and then decrease with the rotation angles. The enclosure with rotation

angle $\alpha = 0^\circ$ has the highest Nusselt number followed by the enclosure with rotation angles $\alpha = 45^\circ$ and $\alpha = 90^\circ$, the enclosure with rotation angle $\alpha = -45^\circ$ has the lowest Nusselt number. Heat conduction becomes playing more and more role when the rotation angle decreases ($\alpha \leq -90^\circ$), and the heat transfer is almost heat conduction when the rotation angle decreases to $\alpha = -90^\circ$. When the hot wall locates in the top and the cold wall locates in the bottom of enclosure ($\alpha = -90^\circ$), the direction of buoyancy is upward, but the top wall prevents the fluid moving upward. The movement of nanofluid in the enclosure is small, and the main heat transfer is the heat conduction, which causes a small Nusselt number. The enclosure with $\alpha = -45^\circ$ is more close to the enclosure with $\alpha = -90^\circ$ and shows the smallest Nusselt number compared with other rotation angles. For the enclosures with rotation angles $\alpha = 45^\circ$ and $\alpha = 90^\circ$, the fluid near the bottom hot wall is heated and moves upward and the fluid near the top cold wall is cooled and moves downward. The directions of hot fluid and cold fluid are opposite and prevent the natural convection heat transfer, which cause a lower Nusselt number compared with the enclosure with $\alpha = 0^\circ$ but a higher Nusselt number compared with the enclosure with $\alpha = -45^\circ$. It can be also seen that the

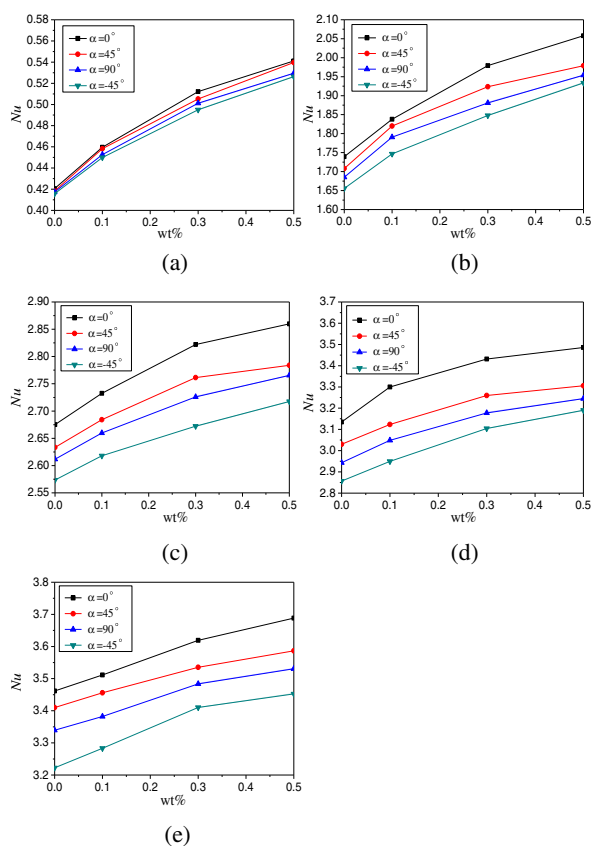


Fig. 9 Changes of Nusselt numbers with nanoparticle mass fractions ($A = 1:2$). Average Nusselt numbers changes of nanofluid in the enclosure ($A = 1:2$) with nanoparticle mass fractions at different heating powers. **a** $Q = 1$ W. **b** $Q = 5$ W. **c** $Q = 10$ W. **d** $Q = 15$ W. **e** $Q = 20$ W

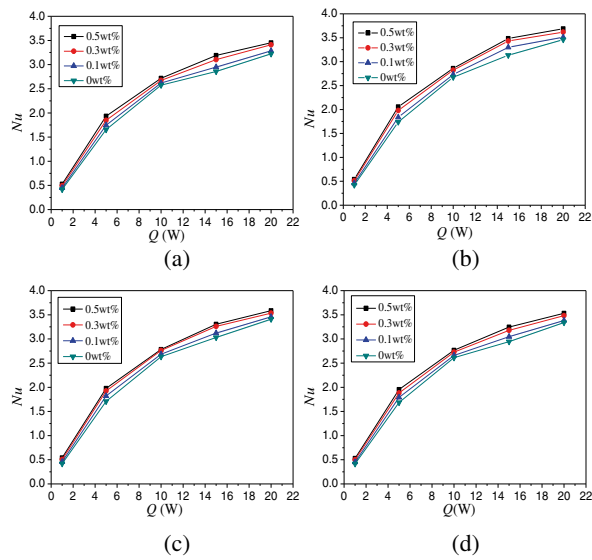


Fig. 10 Changes of Nusselt numbers with heating power ($A = 1:2$). Average Nusselt numbers changes of nanofluid in the enclosure ($A = 1:2$) with heating power at different rotation angles. **a** $\alpha = -45^\circ$. **b** $\alpha = 0^\circ$. **c** $\alpha = 45^\circ$. **d** $\alpha = 90^\circ$

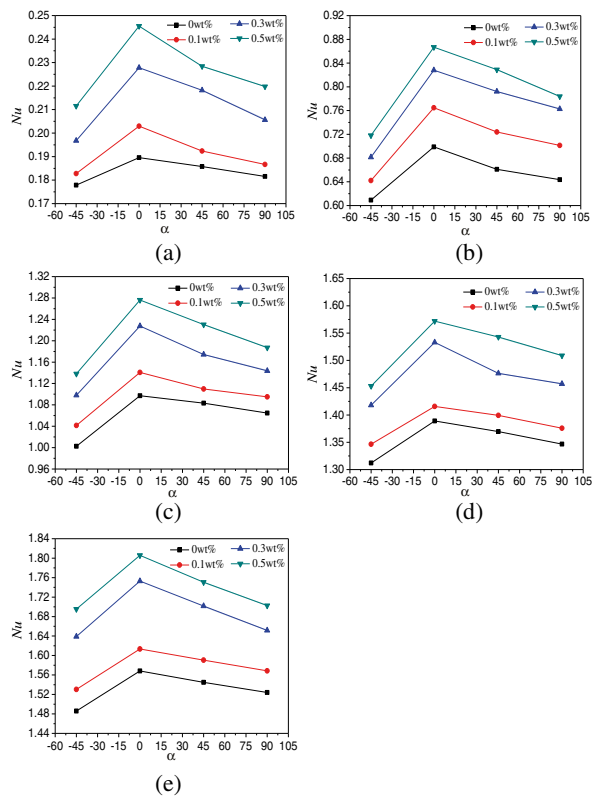


Fig. 11 Changes of Nusselt numbers with rotation angles ($A = 1:4$). Average Nusselt numbers changes of enclosure ($A = 1:4$) at different heating powers. **a** $Q = 1$ W. **b** $Q = 5$ W. **c** $Q = 10$ W. **d** $Q = 15$ W. **e** $Q = 20$ W

differences between various rotation angles increases with the heating power. This is because the effects of rotation angles play the main role on heat transfer at low heating power, and the effects of convective on heat transfer are small. However, the convective heat transfer intensity increases with the heating power and plays the main role on heat transfer at high heating power, which causes the bigger differences between the various rotation angles at high heating power compared with that at low heating power.

In addition to the rotation angles, the effects of nanoparticle mass fraction on the natural convection heat transfer are also discussed. Figure 9 shows the changes of average Nusselt numbers with nanoparticle mass fractions. It can be found that Nusselt numbers increase with nanoparticle mass fractions. For heating power $Q = 1$ W and $\alpha = 0^\circ$, TiO_2 -water nanofluid with wt% = 0.1%, wt% = 0.3%, and wt% = 0.5% can enhance the heat transfer by 9.3, 21.8, and 28.7% compared with water, respectively. The enhancement ratio decreases with the heating power. For heating power $Q = 20$ W and $\alpha = 0^\circ$, TiO_2 -water nanofluid with wt% = 0.1%, wt% = 0.3%, and wt% = 0.5% can enhance the heat transfer by 1.4, 4.6, and 6.6% compared with water, respectively. The

turbulence intensity becomes playing a major role at high heating power, and the effects of nanoparticle mass fraction on heat transfer become small.

The effects of heating powers on the natural convection heat transfer are studied in this paper. Figure 10 shows the changes of average Nusselt numbers with heating power. For $\alpha = 0^\circ$, TiO_2 -water nanofluid at $Q = 5$ W, $Q = 10$ W, $Q = 15$ W, and $Q = 20$ W can enhance the heat transfer by 280.2, 428.4, 544.1, and 581.5% compared with that at $Q = 1$ W. High heating power enhances the turbulence intensity and improves the heat transfer.

Enclosure with $A = 1:4$

In order to investigate the effects of aspect ratios of enclosures on the heat transfer, the natural convection heat transfer characteristics of enclosure with $A = 1:4$ filled with TiO_2 -water nanofluid are studied. Figure 11 gives the changes of average Nusselt numbers with the rotation angles of enclosure. It can be obtained that a similar conclusion like $A = 1:2$ that Nusselt numbers firstly increase and then decrease with the rotation angles. For nanofluid with wt% = 0.5% example, the differences between $A = 1:4$ and $A = 1:2$ are that the enhancement ratios (from 6.5 to 20.7%) of Nusselt number in the enclosure ($A = 1:4, \alpha = 0^\circ$)

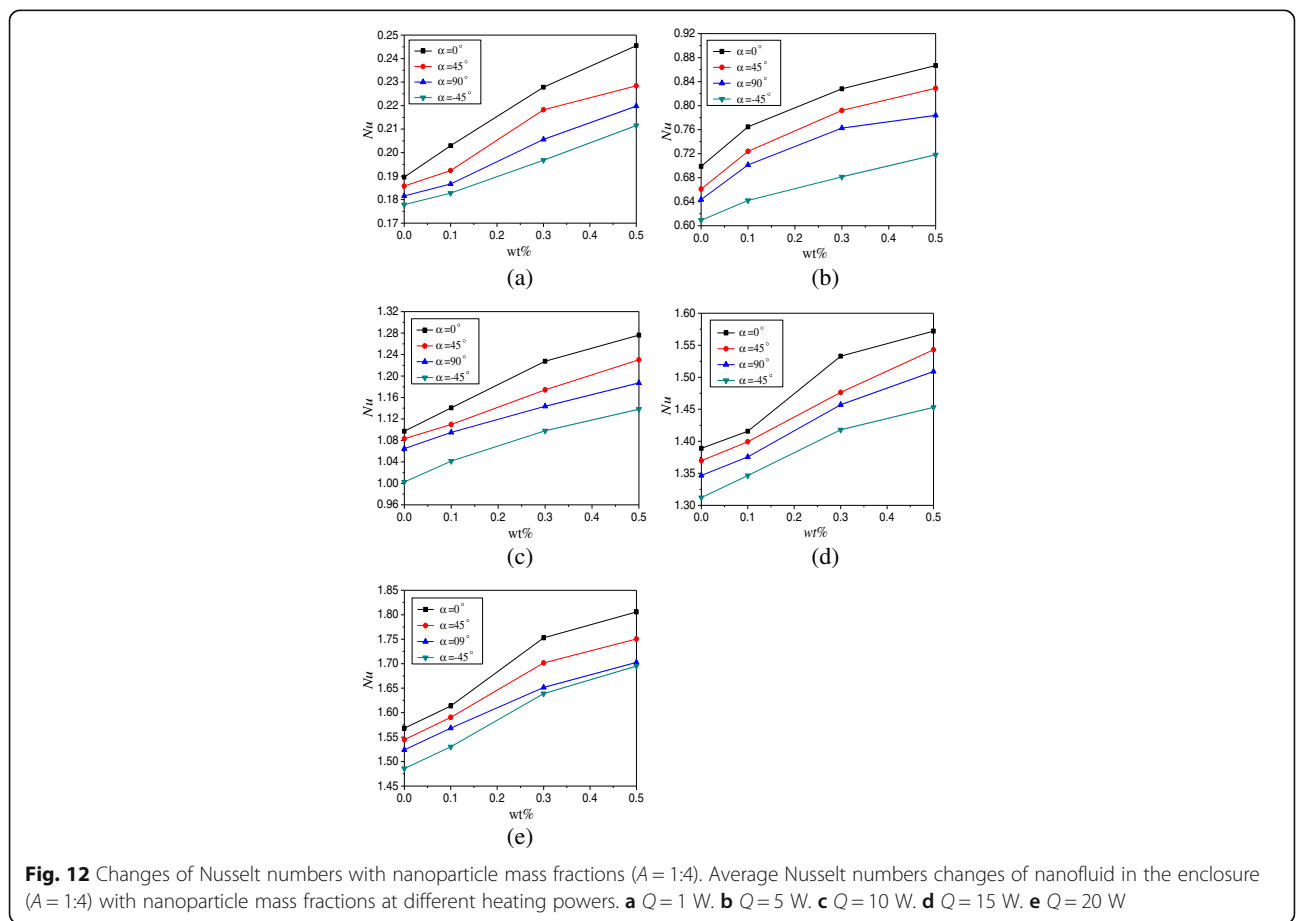


Fig. 12 Changes of Nusselt numbers with nanoparticle mass fractions ($A = 1:4$). Average Nusselt numbers changes of nanofluid in the enclosure ($A = 1:4$) with nanoparticle mass fractions at different heating powers. **a** $Q = 1$ W. **b** $Q = 5$ W. **c** $Q = 10$ W. **d** $Q = 15$ W. **e** $Q = 20$ W

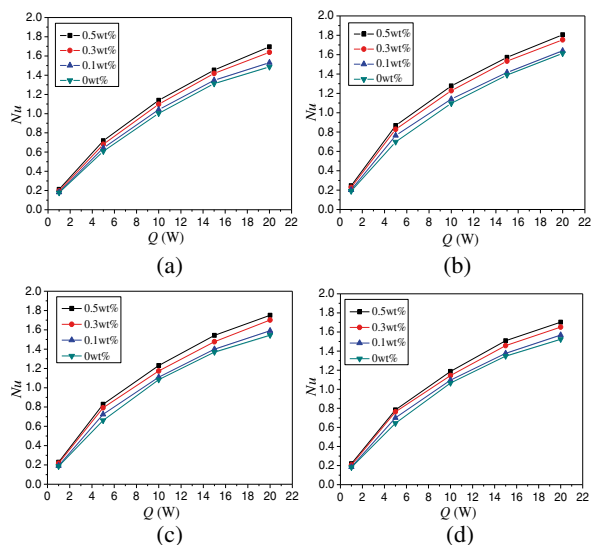


Fig. 13 Changes of Nusselt numbers with heating power ($A = 1:4$). Average Nusselt numbers changes of nanofluid in the enclosure ($A = 1:4$) with heating power at different rotation angles. **a** $\alpha = -45^\circ$. **b** $\alpha = 0^\circ$. **c** $\alpha = 45^\circ$. **d** $\alpha = 90^\circ$

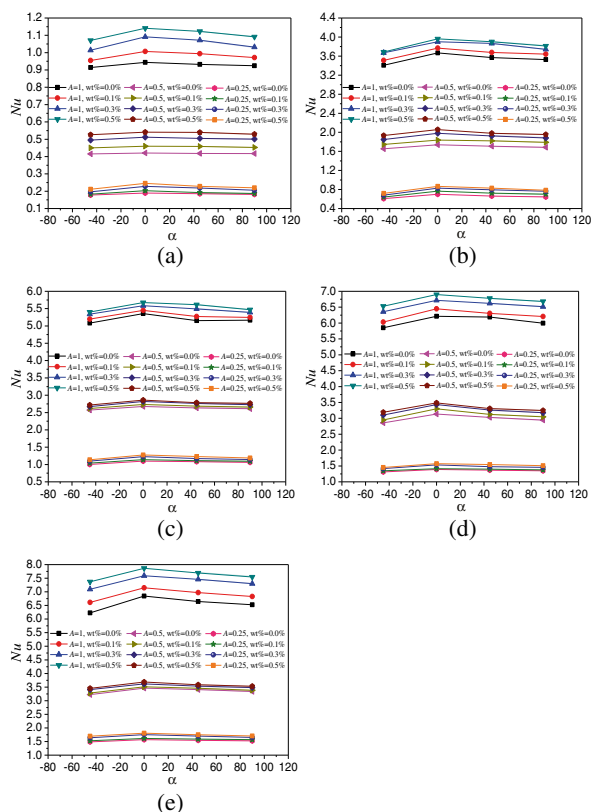


Fig. 14 Nusselt numbers comparison between different aspect ratios. Comparison of average Nusselt numbers of nanofluid in different aspect ratios ($A = 1:1$, $A = 1:2$, and $A = 1:4$) and rotation angle enclosures at different heating powers. **a** $Q = 1$ W. **b** $Q = 5$ W. **c** $Q = 10$ W. **d** $Q = 15$ W. **e** $Q = 20$ W

compared with that in the enclosure ($A = 1:4, \alpha = -45^\circ$) are higher than the enhancement ratios (from 2.85 to 9.3%) of Nusselt number in the enclosure ($A = 1:2, \alpha = 0^\circ$) compared with that in the enclosure ($A = 1:2, \alpha = -45^\circ$).

Figure 12 presents the changes of average Nusselt numbers with nanoparticle mass fractions. For heating power $Q = 1 \text{ W}$ and $\alpha = 0^\circ$, TiO_2 -water nanofluid with $\text{wt}\% = 0.1\%$, $\text{wt}\% = 0.3\%$, and $\text{wt}\% = 0.5\%$ can enhance the heat transfer by 7.1, 20.2, and 29.5% compared with water, respectively. The enhancement ratio decreases with the heating power. For heating power $Q = 20 \text{ W}$ and $\alpha = 0^\circ$, TiO_2 -water nanofluid with $\text{wt}\% = 0.1\%$, $\text{wt}\% = 0.3\%$, and $\text{wt}\% = 0.5\%$ can enhance the heat transfer by 2.9, 11.8, and 15.1% compared with water, respectively.

Figure 13 shows the changes of average Nusselt numbers with heating power. Average Nusselt numbers of nanofluid can be enhanced by 242.4% ~ 701.5% compared with water at heating power $Q = 1 \text{ W}$. For $\alpha = 0^\circ$, TiO_2 -water nanofluid with $\text{wt}\% = 0.5\%$ at $Q = 5 \text{ W}$, $Q = 10 \text{ W}$, $Q = 15 \text{ W}$, and $Q = 20 \text{ W}$ can enhance the heat transfer by 253.0, 419.9, 540.3, and 635.6% compared with that at $Q = 1 \text{ W}$, respectively.

Comparison Between $A = 1:2$, $A = 1:4$, and $A = 1:1$

Due to the length limitation of this paper, the results of enclosure with $A = 1:1$ are only given in Fig. 14, and the effects of different rotation angles, nanoparticle mass fractions, and heating powers on heat transfer can all be shown in Fig. 14. In order to compare the heat transfer characteristics of enclosures with $A = 1:2$, $A = 1:4$, and $A = 1:1$, Fig. 14 shows the comparison of average Nusselt numbers between $A = 1:2$, $A = 1:4$, and $A = 1:1$ at different rotation angles. It is found that the Nusselt numbers increase with the aspect ratio of enclosure. The Nusselt numbers of enclosure ($A = 1:1$ and $A = 1:2$) can be enhanced by 190.6% ~ 224.4% and 103.6% ~ 172.0% compared with the Nusselt numbers of enclosure ($A = 1:4$) at the same conditions, respectively. For $Q = 1 \text{ W}$ and $\alpha = 0^\circ$ example, nanofluid with $\text{wt}\% = 0.5\%$, $\text{wt}\% = 0.3\%$, $\text{wt}\% = 0.1\%$, and $\text{wt}\% = 0.0\%$ in the enclosure with $A = 1:2$ can enhance the heat transfer by 120.4, 124.9, 126.5, and 121.9% compared with that in the enclosure with $A = 1:4$. The enhancement ratio decreases with the heating power. For $Q = 20 \text{ W}$ and $\alpha = 0^\circ$, nanofluid with $\text{wt}\% = 0.5\%$, $\text{wt}\% = 0.3\%$, $\text{wt}\% = 0.1\%$, and $\text{wt}\% = 0.0\%$ in the enclosure with $A = 1:2$ can enhance the heat transfer by 104.2, 106.5, 117.6, 120.7% compared with that in the enclosure with $A = 1:4$. It is also found that Nusselt number increases from $\text{wt}\% = 0.1\%$ to $\text{wt}\% = 0.3\%$ are bigger than that from $\text{wt}\% = 0.3\%$ to $\text{wt}\% = 0.5\%$. This is because the increase of thermal conductivity plays the main role in the heat transfer from $\text{wt}\% = 0.1\%$ to $\text{wt}\% = 0.3\%$, which causes a big enhancement. But the increase of viscosity begins to play the main role in

Table 2 Nusselt numbers ($A = 1:1$). Nusselt number values based on Fig. 14 ($A = 1:1$)

Q	α	Nu (0.5%)	Nu (0.3%)	Nu (0.1%)	Nu (0%)
1 W	-45	1.07043	1.01428	0.95476	0.91431
	0	1.14055	1.09147	1.00692	0.94354
	45	1.12296	1.07193	0.99404	0.93241
	90	1.09139	1.0319	0.97131	0.92421
5 W	-45	3.68552	3.66999	3.50965	3.40783
	0	3.96164	3.90255	3.76721	3.66701
	45	3.90241	3.86575	3.67688	3.56889
	90	3.81346	3.74198	3.64248	3.52605
10 W	-45	5.40131	5.3391	5.19836	5.08178
	0	5.67641	5.58409	5.44825	5.35755
	45	5.61314	5.49212	5.27315	5.15387
	90	5.47057	5.39303	5.24816	5.16605
15 W	-45	6.53082	6.35713	6.03166	5.85206
	0	6.89679	6.71681	6.44823	6.21186
	45	6.7772	6.62197	6.30624	6.18767
	90	6.68041	6.51411	6.20766	5.99525
20 W	-45	7.36842	7.09355	6.61076	6.22726
	0	7.86642	7.59036	7.1488	6.84292
	45	7.69319	7.45785	6.97388	6.64521
	90	7.54729	7.3013	6.82694	6.52435

Table 3 Nusselt numbers ($A = 1:2$). Nusselt number values based on Fig. 14 ($A = 1:2$)

Q	α	Nu(0.5%)	Nu(0.3%)	Nu(0.1%)	Nu(0%)
1 W	-45	0.21153	0.19679	0.18278	0.17788
	0	0.24552	0.22783	0.20294	0.18955
	45	0.2284	0.21822	0.19236	0.18577
	90	0.21981	0.20564	0.18664	0.18157
5 W	-45	0.71806	0.68137	0.64216	0.6091
	0	0.86677	0.82804	0.76474	0.69884
	45	0.829	0.79205	0.72391	0.66098
	90	0.78393	0.76264	0.70126	0.64364
10 W	-45	1.13829	1.09805	1.04143	1.00264
	0	1.27625	1.22757	1.14081	1.09706
	45	1.23027	1.17417	1.10987	1.08314
	90	1.18711	1.14366	1.09506	1.06465
15 W	-45	1.45308	1.41801	1.3465	1.31214
	0	1.572	1.53298	1.41562	1.38905
	45	1.54297	1.47638	1.39931	1.36964
	90	1.50899	1.45712	1.37573	1.34674
20 W	-45	1.69537	1.63891	1.53034	1.48585
	0	1.80587	1.75282	1.61349	1.56828
	45	1.75054	1.70163	1.59055	1.54486
	90	1.70272	1.65153	1.56853	1.52402

Table 4 Nusselt numbers ($A = 1:4$). Nusselt number values based on Fig. 14 ($A = 1:4$)

Q	α	Nu(0.5%)	Nu(0.3%)	Nu(0.1%)	Nu(0%)
1 W	-45	0.5263	0.495	0.44995	0.4157
	0	0.54119	0.51222	0.45962	0.42056
	45	0.53964	0.50517	0.45825	0.4182
	90	0.52953	0.5012	0.45265	0.41729
5 W	-45	1.93363	1.84772	1.74651	1.6555
	0	2.05786	1.97908	1.83774	1.73927
	45	1.97887	1.9236	1.82002	1.70807
	90	1.95401	1.88076	1.79071	1.68525
10 W	-45	2.71752	2.67225	2.61801	2.57357
	0	2.85976	2.82194	2.73248	2.67519
	45	2.78396	2.76133	2.6841	2.63338
	90	2.76545	2.72596	2.65979	2.61159
15 W	-45	3.19016	3.1043	2.94978	2.85708
	0	3.4856	3.43158	3.2998	3.13513
	45	3.3054	3.25965	3.12342	3.03013
	90	3.24525	3.17768	3.0485	2.94331
20 W	-45	3.45233	3.41039	3.28328	3.22254
	0	3.68838	3.61935	3.51132	3.46162
	45	3.58654	3.53537	3.45595	3.40981
	90	3.53074	3.48353	3.38208	3.33931

the heat transfer from $\text{wt}\% = 0.3\%$ to $\text{wt}\% = 0.5\%$, which causes a small enhancement. Because Fig. 14 can cover all the experimental results, the detailed results of Fig. 14 are shown in Tables 2, 3, and 4.

Conclusions

The stability and natural convection heat transfer characteristics of the two enclosures with different rotation angles ($\alpha = -45^\circ$, $\alpha = 0^\circ$, $\alpha = 45^\circ$, and $\alpha = 90^\circ$) filled with TiO_2 -water nanofluid are experimentally investigated. Some conclusions are obtained as follows:

- (1) TiO_2 -water nanofluid with $m = 6 \text{ wt}\%$ and $\text{pH} = 8$ has the lowest transmittance and has the best stability.
- (2) The enclosure with rotation angle $\alpha = 0^\circ$ has the highest Nusselt number followed by the enclosure with rotation angles $\alpha = 45^\circ$ and $\alpha = 90^\circ$; the enclosure with rotation angle $\alpha = -45^\circ$ has the lowest Nusselt number.
- (3) There is a higher heat transfer performance in a bigger aspect ratio enclosure. The Nusselt numbers of enclosure ($A = 1:1$ and $A = 1:2$) can be enhanced by 190.6% ~ 224.4% and 103.6% ~ 172.0% compared with the Nusselt numbers of enclosure ($A = 1:4$) at the same conditions.

(4) Nusselt numbers increase with nanoparticle mass fractions, but the enhancement ratio decreases with the heating power.

(5) Average Nusselt numbers increase with the heating power. Average Nusselt numbers of nanofluid can be enhanced by 701.5% compared with water at the best.

Acknowledgements

This work is financially supported by "National Natural Science Foundation of China" (Grant No. 51606214) and by "the Fundamental Research Funds for the Central Universities" (Grant No. 2015XKMS063).

Authors' contributions

CQ participated in the design of the experiment set and drafted the manuscript. GQW carried out the experiment of nanofluid and processed with the data. YFM and LXG carried out the experiment of nanofluid. All authors read and approved the final manuscript.

Competing interests

The authors declare that they have no competing interests.

Publisher's Note

Springer Nature remains neutral with regard to jurisdictional claims in published maps and institutional affiliations.

Received: 21 March 2017 Accepted: 29 May 2017

Published online: 08 June 2017

References

1. Yang JC, Li FC, Zhou WW, He YR, Jiang BC (2012) Experimental investigation on the thermal conductivity and shear viscosity of viscoelastic-fluid-based nanofluids. *Int J Heat Mass Transfer* 55(11):3160–3166
2. Li FC, Yang JC, Zhou WW, He YR, Huang YM, Jiang BC (2013) Experimental study on the characteristics of thermal conductivity and shear viscosity of viscoelastic-fluid-based nanofluids containing multiwalled carbon nanotubes. *Thermochim Acta* 556:47–53
3. Li H, Wang L, He Y, Hu Y, Zhu J, Jiang B (2015) Experimental investigation of thermal conductivity and viscosity of ethylene glycol based ZnO nanofluids. *Appl Therm Eng* 88:363–368
4. Huang J, He Y, Wang L, Huang Y, Jiang B (2017) Bifunctional Au@TiO₂ core-shell nanoparticle films for clean water generation by photocatalysis and solar evaporation. *Energy Convers Manage* 132:452–459
5. Hu Y, Li H, He Y, Liu Z, Zhao Y (2017) Effect of nanoparticle size and concentration on boiling performance of SiO₂ nanofluid. *Int J Heat Mass Transfer* 107:820–828
6. Chen M, He Y, Huang J, Zhu J (2017) Investigation into Au nanofluids for solar photothermal conversion. *Int J Heat Mass Transfer* 108:1894–1900
7. He Y, Men Y, Zhao Y, Lu H, Ding Y (2009) Numerical investigation into the convective heat transfer of TiO₂ nanofluids flowing through a straight tube under the laminar flow conditions. *Appl Therm Eng* 29(10):1965–1972
8. Sheikholeslami M (2017) Numerical simulation of magnetic nanofluid natural convection in porous media. *Phys Lett A* 381(5):494–503
9. Motlagh SY, Soltanipour H (2017) Natural convection of Al₂O₃-water nanofluid in an inclined cavity using Buongiorno's two-phase model. *Int J Therm Sci* 111:310–320
10. He Y, Qi C, Hu Y, Qin B, Li F, Ding Y (2011) Lattice Boltzmann simulation of alumina-water nanofluid in a square cavity. *Nanoscale Res Lett* 6(1):184–191
11. Qi C, He Y, Yan S, Tian F, Hu Y (2013) Numerical simulation of natural convection in a square enclosure filled with nanofluid using the two-phase Lattice Boltzmann method. *Nanoscale Res Lett* 8(1):56–71
12. Sheikholeslami M, Gorji-Bandpy M, Vajravelu K (2015) Lattice Boltzmann simulation of magnetohydrodynamic natural convection heat transfer of Al₂O₃-water nanofluid in a horizontal cylindrical enclosure with an inner triangular cylinder. *Int J Heat Mass Transfer* 80:16–25
13. Uddin Z, Harmand S (2013) Natural convection heat transfer of nanofluids along a vertical plate embedded in porous medium. *Nanoscale Res Lett* 8(1):1–19

14. Meng X, Li Y (2015) Numerical study of natural convection in a horizontal cylinder filled with water-based alumina nanofluid. *Nanoscale Res Lett* 10(1):142
15. Ahmed M, Eslamian M (2015) Numerical simulation of natural convection of a nanofluid in an inclined heated enclosure using two-phase lattice Boltzmann method: accurate effects of thermophoresis and Brownian forces. *Nanoscale Res Lett* 10(1):296
16. Qi C, He Y, Hu Y, Yang J, Li F, Ding Y (2011) Natural convection of Cu-Gallium nanofluid in enclosures. *J Heat Transfer* 133(12):122504
17. Li H, He Y, Hu Y, Jiang B, Huang Y (2015) Thermophysical and natural convection characteristics of ethylene glycol and water mixture based ZnO nanofluids. *Int J Heat Mass Transfer* 91:385–389
18. Hu Y, He Y, Wang S, Wang Q, Schlager HI (2014) Experimental and numerical investigation on natural convection heat transfer of TiO₂-water nanofluids in a square enclosure. *J Heat Transfer* 136(2):022502
19. Hu Y, He Y, Qi C, Jiang B, Schlager HI (2014) Experimental and numerical study of natural convection in a square enclosure filled with nanofluid. *Int J Heat Mass Transfer* 78:380–392
20. Ho CJ, Liu WK, Chang YS, Lin CC (2010) Natural convection heat transfer of alumina-water nanofluid in vertical square enclosures: an experimental study. *Int J Therm Sci* 49(8):1345–1353
21. Heris SZ, Etemad SG, Esfahany MN (2009) Convective heat transfer of a Cu/water nanofluid flowing through a circular tube. *Exp heat transfer* 22(4):217–227
22. Heris SZ, Esfahany MN, Etemad SG (2007) Experimental investigation of convective heat transfer of Al₂O₃/water nanofluid in circular tube. *Int J Heat Fluid Flow* 28(2):203–210
23. Heris SZ, Etemad SG, Esfahany MN (2006) Experimental investigation of oxide nanofluids laminar flow convective heat transfer. *Int Commun Heat Mass Transfer* 33(4):529–535
24. Mansour RB, Galanis N, Nguyen CT (2011) Experimental study of mixed convection with water-Al₂O₃ nanofluid in inclined tube with uniform wall heat flux. *Int J Therm Sci* 50(3):403–410
25. Chang BH, Mills AF, Hernandez E (2008) Natural convection of microparticle suspensions in thin enclosures. *Int J Heat Mass Transfer* 51(5-6):1332–1341
26. Wen D, Ding Y (2004) Experimental investigation into convective heat transfer of nanofluids at the entrance region under laminar flow conditions. *Int J Heat Mass Transfer* 47(24):5181–5188
27. Wen D, Ding Y (2005) Formulation of nanofluids for natural convective heat transfer applications. *Int J Heat Fluid Flow* 26(6):855–864
28. Li Q, Xuan Y, Wang J (2003) Investigation on convective heat transfer and flow features of nanofluids. *J Heat Transfer* 125:151–155
29. Cioni S, Ciliberto S, Sommeria J (1996) Experimental study of high-Rayleigh-number convection in mercury and water. *Dynam Atmos Oceans* 24(1):117–127

Submit your manuscript to a SpringerOpen[®] journal and benefit from:

- Convenient online submission
- Rigorous peer review
- Open access: articles freely available online
- High visibility within the field
- Retaining the copyright to your article

Submit your next manuscript at ► springeropen.com
